



One Affordable CE Instrument.

*Unlimited Support.
Endless Possibilities.*



The Spectrum Compact CE System offers Sanger Sequencing and 6-dye fragment analysis. With an easy-to-use touch screen, plug-and-play prefilled consumables, compatibility with most data analysis packages and unlimited support, Spectrum Compact has everything you need in one affordable instrument.



Discover the possibilities:

promega.com/SpectrumCompactCE



RESEARCH ARTICLE

A functional platform for the selection of pathogenic variants of *PMM2* amenable to rescue via the use of pharmacological chaperones

Cristina Segovia-Falquina¹ | Alicia Vilas¹ | Fátima Leal¹ |
Francisco del Caño-Ochoa² | Edwin P. Kirk^{3,4} | Magdalena Ugarte¹ |
Santiago Ramón-Maiques^{2,5} | Alejandra Gámez¹  | Belén Pérez¹ 

¹Centro de Diagnóstico de Enfermedades Moleculares, Centro de Biología Molecular-SO UAM-CSIC, Universidad Autónoma de Madrid, Centro de Investigación Biomédica en Red de Enfermedades Raras (CIBERER), Instituto de Investigación Sanitaria IdiPAZ, Madrid, Spain

²Instituto de Biomedicina de Valencia (IBV-CSIC), Valencia, Spain

³School of Women's and Children's Health, University of New South Wales, Randwick, New South Wales, Australia

⁴School of Women's and Children's Health, University of New South Wales, Centre for Clinical Genetics, Sydney Children's Hospital Randwick, NSW Health Pathology East Genomics Laboratory, Randwick, New South Wales, Australia

⁵Instituto de Biomedicina de Valencia (IBV-CSIC), Centro de Investigación Biomédica en Red de Enfermedades Raras (CIBERER-ISCIII), Madrid, Spain

Correspondence

Belén Pérez and Alejandra Gámez, Centro de Diagnóstico de Enfermedades Moleculares, Centro de Biología Molecular, Universidad Autónoma de Madrid, CIBERER, IdiPAZ, Madrid, Spain.

Email: bperez@cbm.csic.es and agamez@cbm.csic.es

Funding information

Instituto de Salud Carlos III; Consejería de Educación, Juventud y Deporte, Comunidad de Madrid; Fundación Isabel Gemio-La Caixa; Fundación Ramón Areces; Australian Government's Medical Research Future Fund

Abstract

Different strategies are being investigated for treating *PMM2*-CDG, the most common congenital disorder of glycosylation. The use of pharmacochaperones (PCs) is one of the most promising. The present work characterizes the expression, stability, and enzymatic properties of 15 previously described clinical variants of the *PMM2* protein, four novel variants, the *Pmm2* mouse variant p.Phe115Leu, and its p.Phe119Leu human counterpart, with the aim of extending the potential use of pharmacochaperoning treatment. *PMM2* variants were purified as stable homodimers, except for p.Asp65Gly, p.Ile120Thr, and p.Thr237Lys (no expression detected), p.Thr226Ser and p.Val231Met (aggregates), and p.Glu93Ala, p.Phe119Leu, and p.Phe115Leu (partial dissociated). Enzyme activity analyses identified severe variants and milder ones. Pure dimeric mutant proteins showed a reduction in thermal stability except for p.Asn216Asp. The thermal stability of all the unstable mutants was recovered in the presence of the PC compound VIII. This study adds to the list of destabilizing human variants amenable to rescue by small chemical compounds that increase the stability/activity of *PMM2*. The proposed platform can be reliably used for assessing the disease-causing effects of *PMM2* missense variants, for assessing the correlation between genotype and phenotype, for confirming new clinical defects, and for identifying destabilizing mutations amenable to rescue by PCs.

KEYWORDS

conformational disease, destabilizing, hypomorphic variant, PCs, *PMM2*, *PMM2*-CDG

This is an open access article under the terms of the Creative Commons Attribution-NonCommercial License, which permits use, distribution and reproduction in any medium, provided the original work is properly cited and is not used for commercial purposes.

© 2022 The Authors. *Human Mutation* published by Wiley Periodicals LLC.

1 | INTRODUCTION

Glycosylation, one of the most common post-translational modifications, allows different proteins and lipids to acquire a glycoconjugate structure and, therefore, function correctly (Cylwik et al., 2013). The process involves the covalent attachment of one or more carbohydrate chains (glycans). Defects in the genes involved in the biosynthesis of glycoconjugates can lead to the disruption of these pathways in different organs, resulting in a heterogeneous group of diseases known as congenital disorders of glycosylation (CDG). PMM2-CDG (MIM# 212065) is the most common. There is no neonatal screening program for it, but its incidence could be as high as 1:20,000 (Jaeken & Matthijs, 2001). PMM2-CDG is caused by the disruption of the N-glycosylation pathway, the consequence of pathogenic variants in the *PMM2* gene (MIM# 601785). The product of this gene is the enzyme phosphomannomutase 2 (PMM2), a homodimeric cytoplasmic protein responsible for the reversible conversion of mannose-6-phosphate into mannose-1-phosphate, a key substrate for N-glycan biosynthesis (Freeze et al., 2014).

PMM2 deficiency causes a variable phenotype ranging from mild to very severe (neonatal death) (Grünewald, 2009). In the vast majority of patients, the nervous system is affected (Jaeken, 2010) by a variety of symptoms including psychomotor delay, cognitive impairment, epilepsy, ataxia, autistic features, strabismus, dysmorphic features, and mild intellectual disability (Verheijen et al., 2020). Other clinical manifestations may include cardiomyopathy, hypotonia, and coagulopathy (Cylwik et al., 2013; Jaeken, 2010). Severe forms are often fatal, with 20% mortality rates reached during the first years of life (Grünewald, 2009). However, patients with only about 25% PMM2 activity in the blood mononuclear cells have been reported to show mild phenotypes, while their carrier parents remain entirely asymptomatic with a minimum of 50% activity (Freeze, 2009; Giurgea et al., 2005).

Of the 130 pathogenic variants identified in *PMM2*, 80% are missense changes according to the Human Gene Mutation Database (HGMD® professional 2021.3). The most common severe European pathogenic variant with null residual PMM2 activity is c.422G>A (p.Arg141His). No patient homozygous for this change has ever been reported (Matthijs et al., 1998) despite carriers being common. This, together with the fact that all *Pmm2* knockout mouse embryos die before birth, suggests homozygous p.Arg141His to be an embryonic lethal genotype (Chan et al., 2016; Matthijs et al., 1998; Schneider et al., 2012) and indicates that the complete lack of PMM2 activity is lethal. The vast majority of patients are compound heterozygous for two different pathogenic variants, the most common genotype involving p.Arg141His and p.Phe119Leu. Since PMM2 activity is essential for life (Kjaergaard et al., 1998; Thiel et al., 2006), compound heterozygous patients with PMM2-CDG must carry at least one hypomorphic pathogenic variant (Vega et al., 2011; Yuste-Checa et al., 2015).

There is no cure for PMM2-CDG, although symptomatic treatments are available (Gámez et al., 2020). A recent example is the repurposed drug AZATA, which can be used to alleviate severe neurological symptoms (Martínez-Monseny et al., 2019). Another is

the aldose reductase inhibitor, Epalrestat, which increases PMM2 activity by preventing glucose from being shunted down the polyol pathway, thus favoring the production of the PMM2 activator glucose-1,6-bisphosphate. It is hoped that Epalrestat will be successful in treating the peripheral neuropathy associated with PMM2-CDG (Ligezka et al., 2021).

Our group has proposed that PMM2-CDG can be understood as a conformational disease, since some missense pathogenic variants destabilize the folding of PMM2 and greatly reduce its activity (Vega et al., 2011; Yuste-Checa et al., 2015). These folding variants have mostly been identified in compound heterozygosity with one severe variant (Vega et al., 2011; Yuste-Checa et al., 2015). We here hypothesize that destabilizing mutations can be rescued by small chemical molecules such as proteostasis regulators (PR) that increase residual PMM2 activity by preventing the protein's degradation or aggregation, and/or by pharmacological chaperones (PCs) that stabilize its defective form (Gámez et al., 2018; Muntau et al., 2014). Indeed, our group has demonstrated the rescue of some folding PMM2 variants by 1-(3-chlorophenyl)-3,3-bis(pyridin-2-yl)-urea (named "compound VIII"). This compound was selected from a library of candidates as capable of stabilizing and/or increasing the activity of several PMM2 pathogenic variants (Yuste-Checa et al., 2017). The results of that work provided the first proof-of-concept that PCs can be used to treat PMM2-CDG, and underpinned the basis for a new therapeutic strategy based on chemically optimized compound VIII.

Recently, our group reported the complete crystal structure of the human PMM2 homodimer (Briso-Montiano et al., 2021). Based on this new knowledge, we proposed the classification of 101 pathogenic missense variants according to their possible damage-causing mechanism. The present work reports an experimental pipeline that, combined with structural analysis, aids in the identification of PMM2 destabilizing hypomorphic variants amenable to rescue by PCs. A set of mutant proteins, most of them found in Spanish patients with PMM2-CDG (and one murine pathogenic variant), was produced in a prokaryotic system and employed in different assays to characterize the effect of the causal mutations on the stability, oligomerization and/or activity of PMM2, and to see whether the damaging effects of any could be reverted by compound VIII. The proposed platform provides a robust basis for the rapid and accurate assessment of potentially disease-causing novel PMM2 variants, and their pathogenic mechanisms. This could be of great assistance in reaching diagnoses and providing genetic counseling to patients with PMM2-CDG.

2 | MATERIALS AND METHODS

The study protocol adhered to the Declaration of Helsinki and was approved by the Ethics Committee of the *Universidad Autónoma de Madrid* on (CEI-CEI-105-2052). Data were collected in accordance with ethical guidelines of each of the institutions involved. Before analysis, written informed consent for genetic testing was obtained from all patients or their legal guardians.

2.1 | Patient genotype selection

The pathogenic variants of interest were selected from Spanish patients with PMM2-CDG recorded in our database, except for variants p.Phe119Leu and p.Ile120Thr (Supporting Information: Table S1). The main requisite for selection was the presence of a severe pathogenic variant with null activity, or its presence in homozygosity. The p.Asn216Asp variant was identified during genetic screening for carriers run as part of the Australian Reproductive Genetic Carrier Screening Project.

2.2 | Structural location of PMM2 pathogenic variants

The structural model of the human PMM2 protein, as well as the location of the residues affected by the selected missense variants was generated using the PyMOL 1.7 Molecular Graphics System (<https://pymol.org/2/>) and the PMM2 crystal coordinates (PDB 7O4G) (Briso-Montiano et al., 2021).

2.3 | Wild-type (wt) PMM2 and pathogenic variant gene expression

The expression plasmid pDEST17-D18 (Source BioScience) encoding human PMM2 cDNA (NM_000303.2), the pReceiver-B01 plasmid encoding mouse *Pmm2* cDNA (NM_016881.3), and the pOPINB expression vector (Briso-Montiano et al., 2021), all with an N-terminal His₆-tag, were used to transform *Escherichia coli* BL21StarTM DE3 One-Shot Cells (Invitrogen). PMM2 pathogenic variants were introduced by site-directed mutagenesis using the QuikChange Lightning Site-Directed Mutagenesis Kit from Agilent Technologies (Santa Clara) and specially designed primers. All products were verified by DNA sequencing.

For protein expression, bacteria were grown overnight at 30°C or 37°C in modified TYM medium (Studier Autoinduction Medium [Studier, 2014] with the N-Z-amine replaced by tryptone) containing 25 µg/ml zeocin, 100 µg/ml ampicillin, or 50 µg/ml kanamycin in the case of pDEST17-D18, pReceiver, and the pOPINB vector, respectively. Cells were harvested by centrifugation. Protein purification and concentration were performed as previously described (Briso-Montiano et al., 2021). Protein concentrations were determined following the Bradford method using Bio-Rad Protein Assay Reagent (Bio-Rad) (Bradford, 1976).

Molecular mass was determined by size-exclusion chromatography coupled to multi-angle light scattering (SEC-MALS) analysis, as described in Briso-Montiano et al. (2021). Data were plotted using GraphPad Prism 6 software.

Protein samples were subjected to electrophoresis in 4%–12% NuPAGE[®] Bis-Tris Precast Gels (Invitrogen). ProSieve[®] Color Protein Markers (Lonza) provided molecular weight markers. Proteins were transferred to a nitrocellulose membrane using the iBlot[®] 2 Dry Blotting System (Invitrogen). Membranes were blocked for at least

1 h with 0.05% phosphate-buffered saline-Tween and 5% low-fat milk. Immunodetection was performed using primary rabbit polyclonal antibody to PMM2 (SAB2702078) (Sigma-Aldrich). Conjugated goat anti-rabbit immunoglobulin G horseradish peroxidase (7074S) (Cell Signaling) was used as the secondary antibody. The Enhanced Chemiluminescence System (GE Healthcare) was used as the detection method. Relative amounts of protein were determined by densitometry using a Bio-Rad GS710 Calibrated Imaging Densitometer running Quantity One v.4.3.1 software (Bio-Rad Laboratories).

2.4 | PMM2 activity assay

The PMM2 activity was assayed using the method of Van Schaftingen (1995), as modified by (de Koning et al., 1998). Assays were performed using 50 ng of purified protein, as quantified by absorbance at 280 nm using the theoretical extinction coefficient of HisPMM2 for the pDEST vector (23,755 M⁻¹ cm⁻¹), for the pOPINB vector (20,775 M⁻¹ cm⁻¹), and for the pReceiver system (23,755 M⁻¹ cm⁻¹). The reaction monitored the increased absorbance at 340 nm due to NADPH production by the coupled reaction (Yuste-Checa et al., 2015).

2.5 | Differential scanning fluorimetry (DSF)

The stability of purified PMM2 mutants was assessed by DSF (Niesen et al., 2007), monitoring thermal denaturation in the presence of the extrinsic fluorescent probe SYPRO Orange (Sigma-Aldrich). This was performed as described elsewhere (Yuste-Checa et al., 2015), and the melting temperature (*T_m*) determined as the temperature at which half of the protein (at relative fluorescence 0.5) was in the unfolded state. Thermal denaturation of all the pathogenic variants was also performed in the presence of compound VIII [1-(3-chlorophenyl)-3, 3-bis(pyridin-2-yl)-urea] (Yuste-Checa et al., 2017) at different concentrations (0, 80, 100, 140, 180, and 200 µM), or in the presence of dimethyl sulfoxide (DMSO) (controls). The results were processed as previously described (Pey et al., 2008).

2.6 | Statistical analysis

Statistical analysis was performed using GraphPad Prism 6 software for Windows. One-way analysis of variance followed by the Dunnett post hoc test was used to compare PMM2 activities and DSF determinations. Data are reported as means ± SD.

3 | RESULTS

3.1 | Selection of variants

The studied variants included 19 human PMM2 missense variants and one murine *Pmm2* variant. Sixteen variants were selected upon

examination of our in-house database of Spanish patients (Supporting Information: Table S1) (Pérez-Cerdá et al., 2017). The selected variants were present in 27 different genotypes. Loss-of-function variants (i.e., premature stop codons, splicing variants) or severe missense variants, such as p.Arg141His or p.Arg123Gln (Briso-Montiano et al., 2021; Yuste-Checa et al., 2015), were not included (Supporting Information: Table S1). Two variants, p.Phe119Leu and p.Ile120Thr, located in the PMM2 dimerization region, and one variant, p.Asn216Asp, identified in an Australian screening program (neither of which have been detected in the Spanish population) were also included. Among the selected variants, p.Asp65Gly, p.Val158Ala, p.Asn216Asp, and p.Thr237Lys have not been reported before. Following ACMG criteria (Richards et al., 2015), they were classified as pathogenic variants. Murine p.Phe115Leu, equivalent to the human pathogenic variant p.Phe119Leu, was also included to determine whether the Pmm2^{p.Phe115Leu/p.Arg137His} mouse is a suitable model for PC analysis.

Together, the selected variants affect seven residues located in the core domain (p.Thr18Ser, p.Tyr64Cys, p.Asp65Gly, p.Asn216Asp, p.Thr226Ser, p.Val231Met, p.Thr237Lys), seven in the cap domain (p.Tyr102Cys, p.Tyr106Phe, p.Val129Met, p.Glu139Lys, p.Ile153Thr, p.Val158Ala, p.Phe183Ser), and five in the dimerization interface (p.Glu93Ala, p.Ala108Val, p.Pro113Leu, p.Phe119Leu, p.Ile120Thr) (Figure 1). The most likely damaging effects of the selected variants were predicted based on the analysis of the recently reported PMM2 structure (Briso-Montiano et al., 2021) (Table 1).

3.2 | Expression of pathogenic variants

Human and murine wt PMM2, and the mutated variants, were produced using a prokaryotic system, employing one of two different expression vectors. Some human variants (p.Thr18Ser, p.Tyr64Cys, p.Asp65Gly, p.Ala108Val, p.Ile153Thr, p.Thr226Ser, and p.Val231Met) were introduced by site-directed mutagenesis into the pDEST17-D18 expression vector (Yuste-Checa et al., 2017), and others (p.Glu93Ala, p.Tyr102Cys, p.Tyr106Phe, p.Pro113Leu, p.Phe119Leu, p.Ile120Thr, p.Val129Met, p.Glu139Lys, p.Val158Ala, p.Phe183Ser, p.Asn216Asp, and p.Thr237Lys) into the pOPINB plasmid (which provides for higher protein expression levels) (Briso-Montiano et al., 2021). The murine variant was introduced into the pReceiver vector. All these vectors add a His-tag at the N-terminus of the protein for affinity purification. The results for each variant were compared with the corresponding human or mouse wt protein obtained using the corresponding vector.

Most pathogenic variants were expressed and isolated at similar purity using a nickel chelating affinity step and size exclusion chromatography (SEC) (Supporting Information: Figures S1 and S2). The exceptions were variants p.Asp65Gly, p.Ile120Thr, and p.Thr237Lys, for which no protein expression could be detected (even by western blot analysis with specific antibodies [data not shown]), irrespective of the vector used or the bacterial growth conditions. Protein expression was recovered upon reversion of

these mutations to the wt sequence (data not shown). These results strongly suggest that mutations p.Asp65Gly, p.Ile120Thr, and p.Thr237Lys severely alter the protein's folding and/or stability.

3.3 | Oligomerization profiles

Next, the effect of the mutations on the oligomeric form of the protein was characterized by SEC. All the pathogenic variants except for p.Glu93Ala eluted in a main peak similar to that shown by the wt protein (Figure 2a and Supporting Information: Figure S1C). A significant fraction (>20%) of the p.Tyr106Phe, p.Val129Met, p.Glu139Lys, p.Val158Ala, p.Phe183Ser, and p.Asn216Asp variants eluted in the void volume of the column, suggesting the formation of large protein aggregates (Table 2). The elution profile of variant p.Glu93Ala showed two peaks, one in the void volume, and a second at a delayed position compared to the protein dimer, suggesting that the mutation disrupts protein dimerization. For the Pmm2 mouse protein, the aggregates represented 21% and 35% of the wt and p.Phe115Leu proteins, respectively, whereas the main peak for both eluted in a delayed position compared to the human wt protein, suggesting the structure of Pmm2 to be more compact than the human form (Figure 2a and Table 2).

The main elution peak for the different proteins was then pooled and analyzed by SEC using a higher resolution column (Superdex 200 Increase 10/300 of 24 ml) coupled to a multiangle light scattering (SEC-MALS) system to obtain accurate measurements of the molecular weight (MW) of the protein oligomers. Most mutants showed a MW of 54 kDa, similar to that of the human protein (Supporting Information: Figure S3), which matches the expected size for the homodimer (Table 2). The mouse wt protein also showed the expected size for a dimer despite the delayed position of the elution peak compared to the human protein. Human p.Glu93Ala and p.Phe119Leu, and the mouse variant p.Phe115Leu, eluted in a delayed position compared to their respective wt proteins (Figure 2c and Supporting Information: Figure S3C) and had MWs lower than expected for a dimer, but higher than the 27 kDa, that would be expected for a monomer (Table 2). These results suggest that mutations p.Glu93Ala and p.Phe119Leu, and the equivalent p.Phe115Leu mutation in Pmm2 mouse, induce the partial dissociation of the protein (an equilibrium between monomers and dimers in solution may exist). In contrast, the estimated MWs of variants p.Thr226Ser and p.Val231Met were higher than expected for a dimer, perhaps due to partial aggregation after SEC (Table 2) (Figure 2b,d), suggesting these two mutants have a severe effect on the folding of the protein.

3.4 | PMM2 enzymatic activity

The enzymatic activities of the wt protein and mutated PMM2 variants eluted in the main peak of the SEC were next measured. Based on the results summarized in Figure 3, the variants were

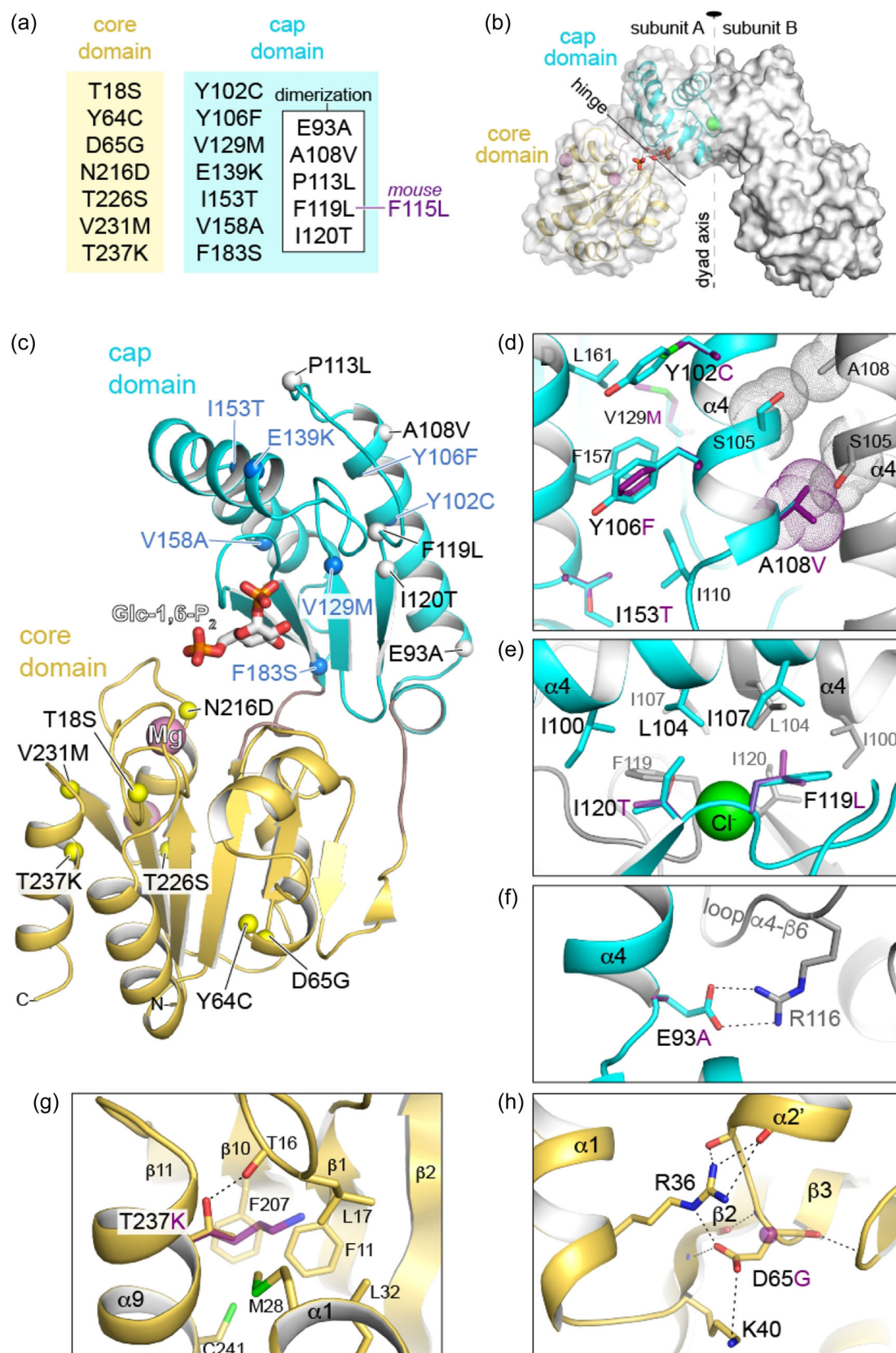


FIGURE 1 (See caption on next page)

classified into two groups, one corresponding to severe mutations with a residual activity of <10% of the wt, which included (in order of increasing activity), p.Phe183Ser, p.Phe115Leu, p.Asn216Asp, p.Glu93Ala, p.Phe119Leu, p.Glu139Lys, p.Tyr64Cys, and p.Ile153Thr, and one corresponding to mutations with a residual activity of >15% of the wt, which included p.Val231Met, p.Pro113Leu, p.Ala108Val, p.Tyr106Phe, p.Tyr102Cys, p.Val129Met, p.Thr226Ser, p.Val158Ala, and p.Thr18Ser. In this last group, the p.Thr18Ser variant stands out for having an activity comparable to that of the wt (Table 2 and Figure 3).

3.5 | PMM2 stability and effect of compound VIII

The thermal stability of the purified PMM2 variants was examined by DSF. The human wt proteins expressed via the plasmids pDEST or pOPINB showed similar melting temperatures (T_m ; $50.6 \pm 0.13^\circ\text{C}$ and $49.9 \pm 0.21^\circ\text{C}$, respectively). All the mutated proteins showed significant instability, with a range of T_m downshifts from 2.3°C to 10.8°C compared to the wt. Variant p.Asn216Asp was an interesting exception, which showed a T_m increase of 2.0°C (Figure 4a) (Table 2).

The most unstable mutant was p.Phe119Leu with a T_m reduction of 10.8°C , followed by, p.Pro113Leu, p.Glu93Ala, p.Ile153Thr, and p.Tyr64Cys, with T_m downshifts from 8.4°C to 7.2°C . p.Tyr102Cys and p.Thr18Ser showed T_m reductions of $<3^\circ\text{C}$. The p.Phe115Leu mouse mutant showed a T_m downshift of 6.8°C compared to the corresponding wt ($T_m = 51.47 \pm 0.12^\circ\text{C}$).

The effect of compound VIII on the thermal stability of the mutants differed. DSF analysis was performed using increasing concentrations of this compound (from 80 to $200 \mu\text{M}$) (Supporting Information: Figure S4). Figure 4b shows the T_m values obtained with the highest concentration of compound VIII assayed ($200 \mu\text{M}$), and in the presence of DMSO as a control. Variant p.Asn216Asp was not further analyzed since its thermal stability was already higher than that of the wt in the absence of compound VIII (Figure 4a). The greatest stabilization effect of compound VIII was observed for p.Glu93Ala, p.Tyr102Cys, and p.Phe119Leu; their T_m were increased by 10°C . Indeed, for these three mutants, together with p.Tyr106Phe, the T_m was similar to, or even higher than, that of the wt reached in the presence of compound VIII. The other mutants also responded positively to the addition of compound VIII, with more moderate increases in stability (Figure 4b and Supporting Information: Figure S4).

The T_m of the p.Phe115Leu mouse variant ($T_m = 44.68 \pm 0.45^\circ\text{C}$; mouse wild type $T_m = 51.47 \pm 0.12^\circ\text{C}$) in the absence of compound VIII was remarkably higher than that of its human counterpart (p.Phe119Leu; $T_m = 39.57 \pm 0.55^\circ\text{C}$). Upon the addition of $200 \mu\text{M}$ of compound VIII, the T_m of p.Phe115Leu increased 3.77°C - still 2°C below the basal T_m of the Pmm2 wt protein but almost 2°C lower than the T_m of p.Phe119Leu in the presence of compound VIII (p.Phe115Leu T_m in the presence of $200 \mu\text{M}$ of compound VIII = $48.74 \pm 0.39^\circ\text{C}$; p.Phe119Leu T_m in the presence of $200 \mu\text{M}$ of compound VIII = $50.68 \pm 0.98^\circ\text{C}$). Thus, the effect of compound VIII on murine p.Phe115Leu appears to be more subtle than on its human counterpart (Figure 4b; Supporting Information: Figure S4).

4 | DISCUSSION

Finding an effective treatment for PMM2-CDG has been a major challenge. Since several pathogenic variants affect PMM2 stability, PMM2-CDG may be considered a misfolding or conformational disease (Vega et al., 2011; Yuste-Checa et al., 2017), and as such is an ideal candidate for being treated with small PCs and/or PRs (Gómez et al., 2018). The structural analysis and biochemical characterization of pathogenic variants may lead to a better understanding of their mechanism of action. This knowledge is essential for detecting PMM2-CDG destabilizing variants, and for determining how many patients with PMM2-CDG might benefit from small molecule therapy.

Only the protein variants p.Asp65Gly, p.Ile120Thr, and p.Thr237Lys could not be produced (under any growth conditions), suggesting that they are severe destabilizing pathogenic variants. One of the most interesting mutants in the core is p.Asp65Gly. The previously characterized p.Asp65Tyr (c.193G>T) mutant (Yuste-Checa et al., 2015) is comparable to p.Asp65Gly in terms of instability, although it retains considerable residual activity (31.9%). Both changes imply the loss of the negatively charged aspartate side chain which is involved in a network of interactions that fastens together different secondary structure elements (Figure 1h and Table 1) (Briso-Montiano et al., 2021). It may be that the substitution of aspartic acid for tyrosine allows some ability to remain involved in these important interactions whereas a mutation to glycine would completely disrupt them (as well as increase the flexibility of the loop containing this residue). Strikingly, p.Asp65Gly has been found in a patient in combination

FIGURE 1 PMM2 dimeric structure and prediction of the effect of the different pathogenic variants. (a) Selected PMM2 variants grouped according to their position in the protein structure. (b) Crystal structure of human PMM2 homodimer (Protein Data Bank accession code 7O4G) shown in surface representation. The surface of one subunit is shown semitransparent in cartoon representation with a bound molecule of glucose 1,6-bisphosphate. The green and pink spheres represent bound Cl^- and Mg^{2+} ions. (c) Representation of the PMM2 subunit with the core and cap domains in yellow and cyan, respectively. The positions affected by mutations shown in (a) are indicated with small spheres. (d-h) Detailed view of residues affected by pathogenic variants. The residues introduced by the mutations are shown in violet to indicate their effect on the surrounding structural elements. In (d) dotted spheres represent the van der Waal radius of selected atoms to show the steric clash of p.Ala108Val with Ser105. In (f, g) dotted lines represent electrostatic interactions disrupted by the pathogenic variants.

TABLE 1 Proposed damaging effects for selected pathogenic missense variants

Core domain	
p.Thr18Ser (c.53C>G)	Thr side chain makes H-bond with loop $\beta 1$ - $\alpha 1$ coordinating the catalytic Mg^{2+} ion. A Ser could maintain the H-bond but reduces hydrophobic interactions, likely altering the active site.
p.Tyr64Cys (c.191A>G)	The Tyr side chain fills the hydrophobic interior of the core domain. A smaller Cys leaves a void and sets a polar group in a hydrophobic environment, destabilizing the core domain.
p.Asp65Gly (c.194A>G)	Asp side chain makes electrostatic interactions between secondary elements of the core domain. A Gly disrupts these interactions increasing flexibility of the loop $\alpha 2'$ - $\beta 3$.
p.Asn216Asp (c.646A>G)	Asn interacts with a water in the coordination sphere of the catalytic Mg^{2+} ion. The negative charge of Asp might interfere with the phosphate transfer reaction by charge repulsion.
p.Thr226Ser (c.677C>G)	Thr coordinates the structural Mg^{2+} ion. A Ser could maintain these interactions but reduces hydrophobic interactions and perhaps distorts the metal coordination.
p.Val231Met (c.691G>A)	Val side chain makes hydrophobic interactions in the interior of the core domain. The larger size of Met would cause steric hindrance.
p.Thr237Lys (c.710C>A)	Thr side chain makes H-bond with loop $\beta 1$ - $\alpha 1$ coordinating the catalytic Mg^{2+} ion. A Lys would cause steric hindrance and places a positive charge within a hydrophobic environment.
Cap domain	
p.Tyr102Cys (c.305A>G)	The Tyr aromatic side-chain makes hydrophobic contacts between helices $\alpha 4$ and $\alpha 6$. The smaller Cys side chain reduces the attraction between them.
p.Tyr106Phe (c.317A>T)	Tyr makes hydrophobic contacts and exposes the phenolic oxygen to the solvent. The missing oxygen in Phe might alter the orientation and interaction between helices $\alpha 4$ and $\alpha 6$.
p.Val129Met (c.385G>A)	The Val side chain faces the hydrophobic cap interior. A Met could cause steric hindrance and likely affect the interaction between Asn128 and the substrate.
p.Glu139Lys (c.415G>A)	The negative Glu side chain likely stabilizes the N-terminal capping of helix $\alpha 5$. The positively charged Lys might disturb this and the position of the helix.
p.Ile153Thr (c.458T>C)	Ile contributes to the hydrophobic interior of the cap domain. A Thr would place a polar side chain in an inappropriate hydrophobic environment.
p.Val158Ala (c.473T>C)	Val contributes to the hydrophobic interior of the cap domain. A smaller Ala would leave a void and reduce hydrophobic contacts.
p.Phe183Ser (c.548T>C)	Phe side chain might interacts with the core domain upon subunit closure. A smaller and polar Ser might alter the subunit movements during the reaction.
Dimerization	
p.Glu93Ala (c.278A>C)	Glu makes a salt bridge with Arg116 across the dimer interface. An Ala would eliminate this strong interaction, reducing the stability of the dimer.
p.Ala108Val (c.323C>T)	Ala side chain in helix $\alpha 4$ projects towards the $\alpha 4$ helix in the other subunit of the dimer. A larger Val would cause steric hindrance across the dimer interface.
p.Pro113Leu (c.338C>T)	Pro introduces a sharp turn between the two principal elements for dimerization ($\alpha 4$ and $\beta 6$). A Leu might alter this proper orientation and reduce dimer stability.
p.Phe119Leu (c.357C>A)	Phe119 is central in the dimerization interface, coordinates the Cl^- ion, and makes hydrophobic contacts. A Leu is the least damaging substitution, but its smaller size and different geometry might alter the interactions across the dimer interface.
p.Ile120Thr (c.359T>C)	Ile120 is central in the dimerization interface, binds the Cl^- ion, and makes hydrophobic contacts. A polar Thr would cause severe distortion of dimerization interface.

with p.Phe157Ser, a variant formerly classified as severe (Vega et al., 2011). Based on the present results, it is here proposed that both variants should be classified as severe. Further experiments with patient cells and recombinant heterodimers (Andreotti et al., 2015) might shed light on the effects of these variants when combined with others.

p.Ile120Thr has been described in different patients in combination with p.Gly228Cys (c.682G>T) (Coorg & Lotze, 2012; Vals et al., 2017) and p.Val231Met (c.691G>A) (Dinopoulos et al., 2007). Both p.Gly228Cys and p.Val231Met are most likely hypomorphic since both are found in combination with the null p.Arg141His variant. In contrast, p.Ile120Thr would appear to be associated with

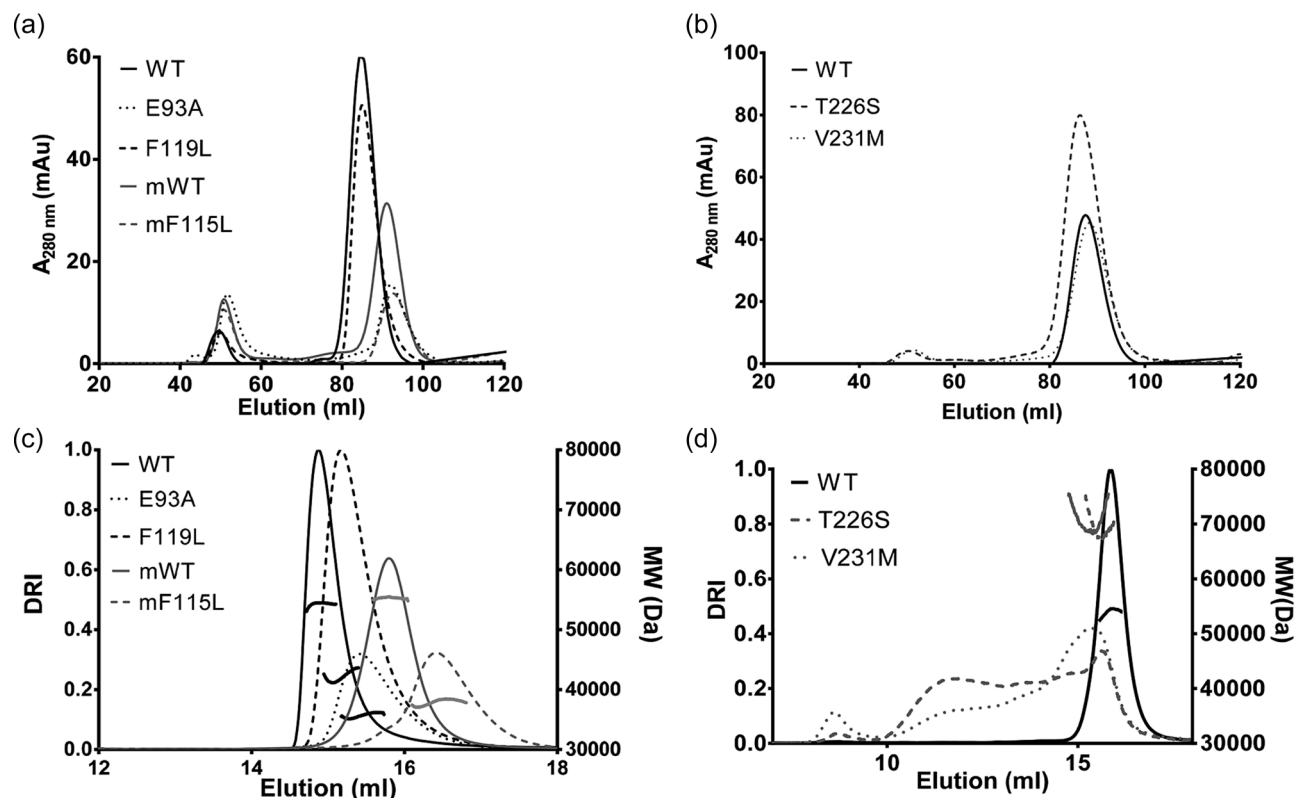


FIGURE 2 Oligomerization profile of representative variants located in the core domain or in the dimerization region of human PMM2 and mouse Pmm2. (a) Size-exclusion chromatograms of the human wt protein (continuous black line), the p.Glu93Ala (pointed black line) and p.Phe119Leu (dashed black line) variants, mouse wt protein (mWT) (continuous gray line), and the p.Phe115Leu variant (dashed gray line). (b) Size-exclusion chromatograms of the human wt protein (continuous black line), and the p.Thr226Ser (dashed gray line) and p.Val231Met (pointed gray line) variants. (c) Oligomerization profile and molecular weight obtained by SEC-MALS for the human wt protein (continuous black line), the p.Glu93Ala (pointed black line) and p.Phe119Leu (dashed black line) variants, the murine wt protein (mWT) (continuous gray line), and the p.Phe115Leu variant (dashed gray line). (d) Oligomerization profile and molecular weight obtained by SEC-MALS for the human wt protein (continuous black line), and the p.Thr226Ser (dashed gray line) and p.Val231Met (pointed gray line) variants. $A_{280\text{ nm}}$, absorbance at 280 nm; DRI, differential refractive index; MW, molecular weight; mAU, mili-absorbance unit; wt, wild-type.

severe loss-of-function. Indeed, several prediction tools anticipate this to be so (Kumar et al., 2021), and the recent revelation of the structure of human PMM2 confirms the central role of Ile120 in protein dimerization (Figure 1e) (Briso-Montiano et al., 2021).

p.Thr237Lys could not be produced under any conditions. Interestingly, a different destabilizing pathogenic variant, p.Thr237Met, was identified in the same residue in earlier work (Yuste-Checa et al., 2015), and its crystal structure showed no crucial differences with respect to the wt protein (Briso-Montiano et al., 2021). These results indicate that whereas the mutation of a threonine to a methionine residue has no great effect on the enzyme's structure, the introduction of a bulky, positively charged lysine residue in the hydrophobic interior of the core domain causes greater protein instability (Figure 1g). In the present patient, the variant with residual activity might have been p.Pro113Leu, a mutation that was found in homozygosity in another patient (Serrano et al., 2015). Overall, these results indicate that p.Asp65Gly, p.Ile120Thr, and p.Thr237Lys can be considered severe pathogenic variants of PMM2, although their precise clinical effects need to be

analyzed in a eukaryotic cellular model due to their degradation mechanisms being different.

All the mutants were less thermally stable than the wt, except for p.Asn216Asp, which had a higher T_m . Analysis of the recently reported structure for PMM2 suggests that Asn216 might participate in catalysis, assisting in the transfer of phosphoryl groups. It is here speculated that the negatively charged side chain of the aspartate replacing Asn216 might mimic the interactions of the phosphate in the active site, perhaps favoring a closed and more stable conformation of the PMM2 subunit. This might explain both the enhanced stability and reduced activity of this mutant. These results indicate that p.Asn216Asp is a severe pathogenic variant.

In general, mutations in the cap domain seem to have a milder effect in terms of activity and thermal stability than do those in the core domain, with some exceptions such as p.Ile153Thr or p.Thr18Ser. The instability and almost total lack of PMM2 activity of p.Ile153Thr may be due to its increased hydrophilicity (Table 1). p.Ile153Thr is found in combination with the loss-of-function variant p.Arg123Ter. Therefore, p.Ile153Thr homodimers must retain some

TABLE 2 Functional analysis results of human PMM2 and mouse Pmm2 mutants and its classification

Pathogenic variants Protein (cDNA)	Aggregates/dimers (%)	MW (KDa) (% error)	Thermal stability ΔT_m (°C) respect to WT ^a	Enzymatic activity in pure protein (%)
PMM2				
WT (-)	9/91	54.3 (8%)	-	100
Core domain				
p.Thr18Ser (c.53C>G)	1.3/98.7	54.8 (8%)	-2.92 ± 0.12***	99.36 ± 16.53 ^{n.s.}
p.Tyr64Cys (c.191A>G)	3.5/96.5	55.6 (8%)	-7.16 ± 0.15***	8.06 ± 3.58***
p.Asp65Gly (c.194A>G)	n.d.	n.d.	n.d.	n.d.
p.Asn216Asp (c.646A>G)	36.5/63.5	-	+2.09 ± 0.68***	2.94 ± 1.41***
p.Thr226Ser (c.677C>G)	2.3/97.7	71.1 (9%)	-5.04 ± 0.15***	55.6 ± 14.52**
p.Val231Met (c.691G>A)	4/96	70.6 (8%)	-6.0 ± 0.28***	18.44 ± 5.48***
p.Thr237Lys (c.710C>A)	n.d.	n.d.	n.d.	n.d.
Cap domain				
p.Tyr102Cys (c.305A>G)	13.1/86.9	52.9 (0.8%)	-2.26 ± 0.75***	43.3 ± 1.48***
p.Tyr106Phe (c.317A>T)	37.8/62.2	52.4 (1%)	-5.58 ± 1.02***	38.5 ± 2.08***
p.Val129Met (c.385G>A)	23.9/76.1	55.9 (8%)	-4.69 ± 0.38***	46.28 ± 5.61***
p.Glu139Lys (c.415G>A)	22.4/77.6	51.8 (2%)	-4.68 ± 0.38***	7.35 ± 2.42***
p.Ile153Thr (c.458T>C)	5.9/94.1	57.2 (8%)	-7.28 ± 0.21***	8.37 ± 2.24***
p.Val158Ala (c.473T>C)	24.8/75.2	55.7 (8%)	-5.58 ± 0.38***	63.84 ± 6.78***
p.Phe183Ser (c.548T>C)	21.5/78.5	57.2 (8%)	-3.78 ± 0.38***	2.07 ± 3.08***
Dimerization interface				
p.Glu93Ala (c.278A>C)	41.3/58.7	35.8 (2%)	-7.98 ± 0.87***	3.6 ± 0.85***
p.Ala108Val (c.323C>T)	2.9/97.1	56.6 (8%)	-5.19 ± 0.13***	36.86 ± 9.09***
p.Pro113Leu (c.338C>T)	15.8/84.2	52.5 (8%)	-8.39 ± 0.76***	19.2 ± 4.87***
p.Phe119Leu (c.357C>A)	8/92	42.6 (8%)	-10.75 ± 0.81***	4.95 ± 1.63***
p.Ile120Thr (c.359T>C)	n.d.	n.d.	n.d.	n.d.
Pmm2				
WT (-)	21/79	55.3 (8%)	-	100
p.Phe115Leu (c.345C>A)	35.1/64.9	37.9 (8%)	-6.79 ± 0.46***	2.2 ± 0.6***

Note: Nucleotide numbering uses +1 as the A of the ATG translation initiation codon in the reference sequence, with the initiation codon as codon 1. All mutations have been checked using the Mutalyzer program. PMM2 (NM_000303.2); Pmm2 (NM_016881.2). The error of the MW determination is expressed as the percentage (%) of the measures that differ from the widespread value. In bold it is highlighted the most significant and relevant results when compared to the wild-type values.

Abbreviations: Aggr., aggregates; MW, molecular weight; n.d., not determined; n.s., not significant; T_m , melting temperature; WT, wild type.

^a T_m of human WT (pDEST T_m : 50.6 ± 0.13°C, pOPINB T_m : 49.91 ± 0.21°C), T_m of mouse WT (51.47 ± 0.12°C).

*** p < 0.001; ** p < 0.01; * p < 0.05.

residual activity in patients' cells. The residual enzymatic activity of the previously described p.Thr18Ser is similar to that of the wt, raising the question of whether this mutation is really pathogenic at all. p.Thr18Ser was found in combination with p.Arg141His in one of the present Spanish patients, in whom no other variants in the exomic region of PMM2 were found, although it cannot be ruled out that undetected mutations affect the gene's expression. Based on its structural analysis, mutation p.Thr18Ser is likely a conservative

change since both threonine and serine are polar amino acids (Table 1). The mild effects that were observed for p.Thr18Ser agree with results described in another bacterial system (Le Bizet et al., 2005). Further expression analysis should be performed to determine the pathogenicity of this variant.

The behavior of the variants p.Tyr64Cys and p.Glu139Lys, which were found in homozygosity (Supporting Information: Table S1 and Table 1), is remarkable. p.Tyr64Cys was previously thought to have a

mild or moderate effect since it was found in homozygosity or in combination with p.Arg141His (Briones et al., 2002). However, the present results, and predictions made by other authors (Kumar et al., 2021), indicate it to be a severe pathogenic variant. As reported for other inherited metabolic diseases, several factors including the variant present in the other allele, the genetic background, plus epigenetic and environmental factors (Scriver & Waters, 1999), will need to be taken into account if we are to better understand the pathophysiology of PMM2-CDG. Similarly, and despite its low

activity, the p.Glu139Lys variant was found both in homozygosity and in combination with the severe folding variant p.Phe207Ser, previously characterized by Yuste-Checa et al. (2015). This variant was previously proposed to alter PMM2 mRNA splicing (Vuillaumier-Barrot et al., 1999); this could lead to phenotype modifications.

Five of the studied pathogenic variants locate to the dimerization interface (Table 1), but according to the present results, only p.Glu93Ala, p.Phe119Leu (or its murine homolog p.Phe115Leu), and p.Ile120Thr can be truly classified as dimerization variants (Table 2). p.Glu93Ala and p.Phe119Leu were in combination with p.Arg141His, indicating that the latter can dimerize with these variants, and p.Ile120Thr has been described in combination with the likely milder variant p.Gly228Cys (Coorg & Lotze, 2012; Vals et al., 2017). Crystal structure analysis of Phe119 and Ile120 showed that they interact with a Cl^- ion located on the dimerization interface (Table 1) (Briso-Montiano et al., 2021). Whereas p.Ile120Thr could not be expressed, both p.Glu93Ala or p.Phe119Leu hampered protein dimerization (Figure 2a,c), and the mutated proteins in solution were in an equilibrium between monomeric and dimeric forms irresolvable by SEC. Variants p.Glu93Ala and p.Phe119Leu might alter the dimerization interface, causing the exposure of the hydrophobic residues involved in this region and, therefore, disrupt the overall native structure. The presence of p.Phe119Leu or p.Glu93Ala in combination with p.Arg141His, or even of p.Phe119Leu in homozygosity, suggests that these variants have a milder effect on dimerization than p.Ile120Thr. The present results show that the mouse variant p.Phe115Leu has an impact similar to that of the human variant p.Phe119Leu, suggesting Pmm2 p.Phe115Leu/p.Arg137His mice to be a suitable model for testing PCs in vivo. It is remarkable that mutations p.Ala108Val and p.Pro113Leu do not alter the dimeric nature of PMM2. It is possible that the high protein concentrations used for SEC and SEC-MALS favor the formation of protein dimers,

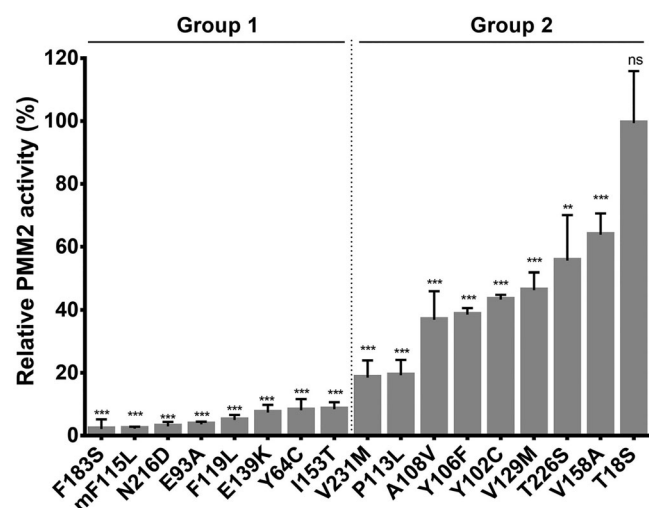


FIGURE 3 PMM enzymatic activity. Relative PMM activity of pure protein. Wild-type activity represents 100%. Group 1: mutants with very low residual activity (<10% compared to the wild type). Group 2: mutants with high residual activity (>15% compared to the wild type). The data represent the mean \pm SD of at least three independent experiments (ns, not significant; *** p < 0.001; ** p < 0.01, * p < 0.05).

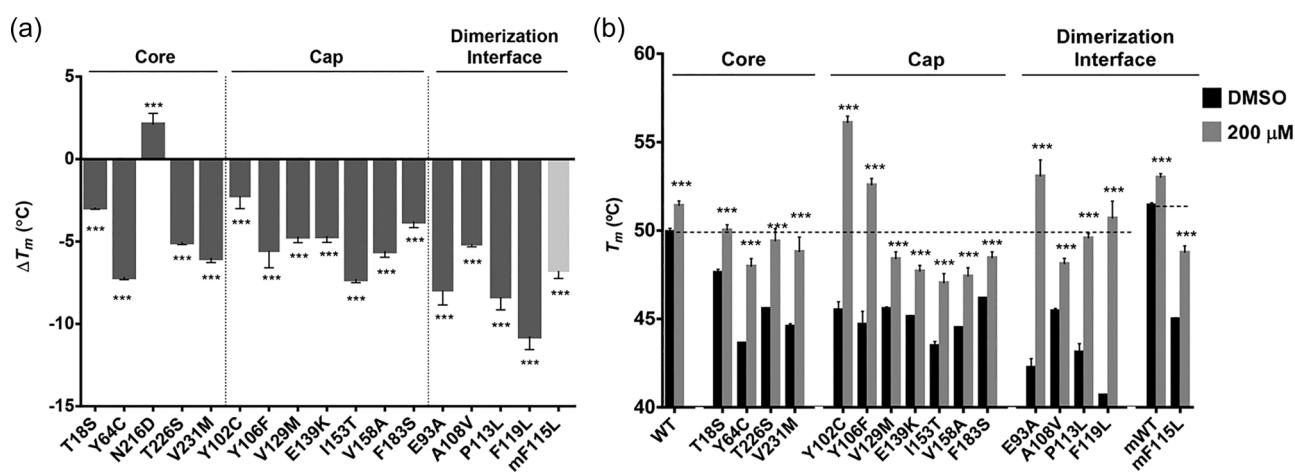


FIGURE 4 Thermal stability analysis. (a) Effect of the PMM2 pathogenic variants on thermal stability, as determined by DSF. The increase in T_m is reported as ΔT_m (°C) for each pathogenic variant compared to the wt T_m value. (b) Effect of 200 μM compound VIII on the thermal stability of PMM2 mutants. The increase in T_m (°C) after the treatment with 200 μM compound VIII (grey) is compared with the T_m of each mutant in the presence of DMSO (black). The dashed line indicates the T_m of the wt PMM2 protein with DMSO. The variants are classified according to their structural location. The data represent the mean \pm SD of at least three independent experiments (ns, not significant; *** p < 0.001; ** p < 0.01, * p < 0.05). DMSO, dimethyl sulfoxide; DSF, differential scanning fluorimetry.

but at the low concentrations used in the activity assays, the protein was partially dissociated and retained only 20%–40% of wt activity (Table 2).

The proposed platform provides an accurate and rapid means of assessing variants of unknown clinical significance, allowing for improved genetic counseling. The results show the pathogenic effect of the unreported variant p.Asn216Asp. This variant was identified in one member of a couple (the other had p.Arg141His) during a genetic screening program in Australia. Based on the analysis of its structure, and on the other experimental data presented in the present work, we propose that the lack of enzyme activity in this mutant is owed to the importance of Asn216 in properly positioning the catalytic residue Asp209 and the Mg^{2+} cofactor in the active site (Briso-Montiano et al., 2021). Undoubtedly, the remarkable expansion of genomic technologies to carrier and neonatal screening programs will increase the number of variants of uncertain significance known, and increase the importance of the availability of a functional platform in rapidly returning accurate results.

The results show that 15 human PMM2 pathogenic variants obtained in this prokaryotic system, in addition to the murine mutant, are destabilizing, hypomorphic variants amenable to rescue by small molecules, and three are probably severe destabilizing mutants. In addition—and as described for other conformational diseases such as MCADD (Jank et al., 2014)—fever may be a crucial risk factor for metabolic decompensation in patients with destabilizing mutations in PMM2. Early antipyretic treatment should therefore be considered.

A strategy combining both PCs and PRs might result in the recovery of the native structure of mutants that retain some enzymatic activity, despite their tendency to aggregate (Mu et al., 2008; Vilas et al., 2020). Future perspectives include using cellular disease models (differentiated from induced pluripotent stem cells) for testing the effectiveness of compound VIII and its chemical derivatives. Epalrestat is an activator of PMM2 activity, but it does not increase the stability of the protein as does compound VIII. However, both target destabilizing variants that retain some residual activity. The present results therefore also suggest that Epalrestat could be given to many patients with PMM2-CDG; in combination with PCs any beneficial effect may be greater.

In combination with the structural information recently described for PMM2 crystals (Briso-Montiano et al., 2021), the present work suggests that many patients could be treated using small chemical molecules that increase the concentration of working PMM2.

ACKNOWLEDGMENTS

We wholeheartedly thank the Spanish families affected by PMM2-CDG who participated in this study. This study was funded by the *Fundación Isabel Gemio-Fundación La Caixa* [LCF/PR/PR16/11110018], the *Instituto de Salud Carlos* (ISCIII), the European Regional Development Fund [PI19/01155], the *Consejería de Educación, Juventud y Deporte, Comunidad de Madrid* [B2017/BMD3721], and the *Fundación Ramón Areces Ciencias de la Vida* (XX National Call). The Australian Reproductive Genetic Carrier Screening Project is funded by the Australian Government's Medical Research Future

Fund as part of the Australian Genomics Health Futures Mission (GHFM73390 [MRFF-G-MM]).

CONFLICT OF INTEREST

The author declares no conflict of interest.

DATA AVAILABILITY STATEMENT

The data that support the findings of this study are available from the corresponding author upon reasonable request.

The data for the new variants described in this study are included in LOVD (<https://www.lovd.nl/>) with the reference numbers 0000868533, 0000868535, 0000868539, and 0000868541.

WEB SOURCES

<http://varnomen.hgvs.org/bg-material/refseq/>

<https://mutalyzer.nl>

<http://www.omim.org>

<https://www.ensembl.org/index.html>

ORCID

Alejandra Gámez  <https://orcid.org/0000-0002-2414-2586>

Belén Pérez  <http://orcid.org/0000-0002-3190-1958>

REFERENCES

- Andreotti, G., Monti, M. C., Citro, V., & Cubellis, M. V. (2015). Heterodimerization of two pathological mutants enhances the activity of human Phosphomannomutase2. *PLoS One*, 10(10), e0139882. <https://doi.org/10.1371/journal.pone.0139882>
- Bradford, M. M. (1976). A rapid and sensitive method for the quantitation of microgram quantities of protein utilizing the principle of protein-dye binding. *Analytical Biochemistry*, 72, 248–254. <https://doi.org/10.1006/abio.1976.9999>
- Briones, P., Vilaseca, M. A., Schollen, E., Ferrer, I., Maties, M., Busquets, C., Artuch, R., Gort, L., Marco, M., Schaftingen, E. V., Matthijs, G., Jaeken, J., & Chaba, A. (2002). Biochemical and molecular studies in 26 Spanish patients with congenital disorder of glycosylation type Ia. *Journal of Inherited Metabolic Disease*, 25(8), 635–646. <https://doi.org/10.1023/a:1022825113506>
- Briso-Montiano, A., Del Caño-Ochoa, F., Vilas, A., Velázquez-Campoy, A., Rubio, V., Pérez, B., & Ramón-Maiques, S. (2021). Insight on molecular pathogenesis and pharmacochaperoning potential in phosphomannomutase 2 deficiency, provided by novel human phosphomannomutase 2 structures. *Journal of Inherited Metabolic Disease*, 45, 318–333. <https://doi.org/10.1002/jimd.12461>
- Chan, B., Clasquin, M., Smolen, G. A., Histen, G., Powe, J., Chen, Y., Lin, Z., Lu, C., Liu, Y., Cang, Y., Yan, Z., Xia, Y., Thompson, R., Singleton, C., Dorsch, M., Silverman, L., Su, S.-S. M., Freeze, H. H., & Jin, S. (2016). A mouse model of a human congenital disorder of glycosylation caused by loss of PMM2. *Human Molecular Genetics*, 25(11), 2182–2193. <https://doi.org/10.1093/hmg/ddw085>
- Coorg, R., & Lotze, T. E. (2012). Child neurology: A case of PMM2-CDG (CDG 1a) presenting with unusual eye movements. *Neurology*, 79(15), e131–e133. <https://doi.org/10.1212/WNL.0b013e31826e2617>
- Cylwik, B., Naklicki, M., Chrostek, L., & Gruszevska, E. (2013). Congenital disorders of glycosylation. part I. Defects of protein N-glycosylation. *Acta Biochimica Polonica*, 60(2), 151–161. <https://doi.org/10.18388/abp.2013.1965>
- de Koning, T. J., Dorland, L., van Diggelen, O. P., Boonman, A. M. C., de Jong, G. J., van Noort, W. L., De Schryver, J., Duran, M.,

- van den Berg, I. E. T., Gerwig, G. J., Berger, R., & Poll-The, B. T. (1998). A novel disorder of N-glycosylation due to phosphomannose isomerase deficiency. *Biochemical and Biophysical Research Communications*, 245(1), 38–42. <https://doi.org/10.1006/bbrc.1998.8385>
- Dinopoulos, A., Mohamed, I., Jones, B., Rao, S., Franz, D., & de Grauw, T. (2007). Radiologic and neurophysiologic aspects of stroke-like episodes in children with congenital disorder of glycosylation type Ia. *Pediatrics*, 119(3), e768–e772. <https://doi.org/10.1542/peds.2006-0763>
- Freeze, H. H. (2009). Towards a therapy for phosphomannomutase 2 deficiency, the defect in CDG-Ia patients. *Biochimica et Biophysica Acta (BBA)—Molecular Basis of Disease*, 1792(9), 835–840. <https://doi.org/10.1016/j.bbadis.2009.01.004>
- Freeze, H. H., Chong, J. X., Bamshad, M. J., & Ng, B. G. (2014). Solving glycosylation disorders: Fundamental approaches reveal complicated pathways. *The American Journal of Human Genetics*, 94(2), 161–175. <https://doi.org/10.1016/j.ajhg.2013.10.024>
- Gámez, A., Serrano, M., Gallego, D., Vilas, A., & Pérez, B. (2020). New and potential strategies for the treatment of PMM2-CDG. *Biochimica et Biophysica Acta (BBA)—General Subjects*, 1864(11), 129686. <https://doi.org/10.1016/j.bbagen.2020.129686>
- Gámez, A., Yuste-Checa, P., Brasil, S., Briso-Montiano, Á., Desviat, L. R., Ugarte, M., Pérez-Cerdá, C., & Pérez, B. (2018). Protein misfolding diseases: Prospects of pharmacological treatment. *Clinical Genetics*, 93(3), 450–458. <https://doi.org/10.1111/cge.13088>
- Giurgea, I., Michel, A., Le Merrer, M., Seta, N., & de Lonlay, P. (2005). Underdiagnosis of mild congenital disorders of glycosylation type Ia. *Pediatric Neurology*, 32(2), 121–123. <https://doi.org/10.1016/j.pediatrneurol.2004.06.021>
- Grünwald, S. (2009). The clinical spectrum of phosphomannomutase 2 deficiency (CDG-Ia). *Biochimica et Biophysica Acta (BBA)—Molecular Basis of Disease*, 1792(9), 827–834. <https://doi.org/10.1016/j.bbadis.2009.01.003>
- Jaeken, J. (2010). Congenital disorders of glycosylation: Congenital disorders of glycosylation. *Annals of the New York Academy of Sciences*, 1214(1), 190–198. <https://doi.org/10.1111/j.1749-6632.2010.05840.x>
- Jaeken, J., & Matthijs, G. (2001). Congenital disorders of glycosylation. *Annual Review of Genomics and Human Genetics*, 2001(2), 129–151.
- Jank, J. M., Maier, E. M., Reiß, D. D., Haslbeck, M., Kemter, K. F., Truger, M. S., Sommerhoff, C. P., Ferdinandusse, S., Wanders, R. J., Gersting, S. W., & Muntau, A. C. (2014). The domain-specific and temperature-dependent protein misfolding phenotype of variant medium-chain acyl-CoA dehydrogenase. *PLoS One*, 9(4), e93852. <https://doi.org/10.1371/journal.pone.0093852>
- Kjaergaard, S., Skovby, F., & Schwartz, M. (1998). Absence of homozygosity for predominant mutations in PMM2 in Danish patients with carbohydrate-deficient glycoprotein syndrome type 1. *European Journal of Human Genetics*, 6(4), 331–336. <https://doi.org/10.1038/sj.ejhg.5200194>
- Kumar, D., Jain, N., Udhaya Kumar, S., George Priya Doss, C., & Zayed, H. (2021). Identification of potential inhibitors against pathogenic missense mutations of PMM2 using a structure-based virtual screening approach. *Journal of Biomolecular Structure and Dynamics*, 39(1), 171–187. <https://doi.org/10.1080/07391102.2019.1708797>
- Le Bizet, C., Vuillaumier-Barrot, S., Barnier, A., Dupré, T., Durand, G., & Seta, N. (2005). A new insight into PMM2 mutations in the French population. *Human Mutation*, 25(5), 504–505. <https://doi.org/10.1002/humu.9336>
- Ligezka, A. N., Radenkovic, S., Saraswat, M., Garapati, K., Ranatunga, W., Krzysciak, W., Yanaiharu, H., Preston, G., Brucker, W., McGovern, R. M., Reid, J. M., Cassiman, D., Muthusamy, K., Johnsen, C., Mercimek-Andrews, S., Larson, A., Lam, C., Edmondson, A. C., Ghesquière, B., ... Morava, E. (2021). Sorbitol is a severity biomarker for PMM2-CDG with therapeutic implications. *Annals of Neurology*, 90(6), 887–900. <https://doi.org/10.1002/ana.26245>
- Martínez-Monseny, A. F., Bolasell, M., Callejón-Póo, L., Cuadras, D., Freniche, V., Itzep, D. C., Gassiot, S., Arango, P., Casas-Alba, D., de la Morena, E., Corral, J., Montero, R., Pérez-Cerdá, C., Pérez, B., Artuch, R., Jaeken, J., Serrano, M., & CDG Spanish Consortium. (2019). AZATA: Acetazolamide safety and efficacy in cerebellar syndrome in PMM2 congenital disorder of glycosylation (PMM2-CDG). *Annals of Neurology*, 85(5), 740–751. <https://doi.org/10.1002/ana.25457>
- Matthijs, G., Schollen, E., Van Schaftingen, E., Cassiman, J.-J., & Jaeken, J. (1998). Lack of homozygotes for the most frequent disease allele in carbohydrate-deficient glycoprotein syndrome type 1A. *The American Journal of Human Genetics*, 62(3), 542–550. <https://doi.org/10.1086/301763>
- Mu, T.-W., Ong, D. S. T., Wang, Y.-J., Balch, W. E., Yates, J. R., Segatori, L., & Kelly, J. W. (2008). Chemical and biological approaches synergize to ameliorate protein-folding diseases. *Cell*, 134(5), 769–781. <https://doi.org/10.1016/j.cell.2008.06.037>
- Muntau, A. C., Leandro, J., Staudigl, M., Mayer, F., & Gersting, S. W. (2014). Innovative strategies to treat protein misfolding in inborn errors of metabolism: Pharmacological chaperones and proteostasis regulators. *Journal of Inherited Metabolic Disease*, 37(4), 505–523. <https://doi.org/10.1007/s10545-014-9701-z>
- Niesen, F. H., Berglund, H., & Vedadi, M. (2007). The use of differential scanning fluorimetry to detect ligand interactions that promote protein stability. *Nature Protocols*, 2(9), 2212–2221. <https://doi.org/10.1038/nprot.2007.321>
- Pérez-Cerdá, C., Girós, M. L., Serrano, M., Ecay, M. J., Gort, L., Pérez Dueñas, B., Medrano, C., García-Alix, A., Artuch, R., Briones, P., & Pérez, B. (2017). A population-based study on congenital disorders of protein N- and combined with O-Glycosylation experience in clinical and genetic diagnosis. *The Journal of Pediatrics*, 183, 170–177. <https://doi.org/10.1016/j.jpeds.2016.12.060>
- Pey, A. L., Ying, M., Cremades, N., Velazquez-Campoy, A., Scherer, T., Thöny, B., Sancho, J., & Martinez, A. (2008). Identification of pharmacological chaperones as potential therapeutic agents to treat phenylketonuria. *Journal of Clinical Investigation*, 118(8), 2858–2867. <https://doi.org/10.1172/JCI34355>
- Richards, S., Aziz, N., Bale, S., Bick, D., Das, S., Gastier-Foster, J., Grody, W. W., Hegde, M., Lyon, E., Spector, E., Voelkerding, K., & Rehman, H. L. (2015). Standards and guidelines for the interpretation of sequence variants: A joint consensus recommendation of the American College of Medical Genetics and genomics and the Association for Molecular Pathology. *Genetics in Medicine*, 17(5), 405–423. <https://doi.org/10.1038/gim.2015.30>
- Schneider, A., Thiel, C., Rindermann, J., DeRossi, C., Popovici, D., Hoffmann, G. F., Gröne, H.-J., & Körner, C. (2012). Successful prenatal mannose treatment for congenital disorder of glycosylation-Ia in mice. *Nature Medicine*, 18(1), 71–73. <https://doi.org/10.1038/nm.2548>
- Scriver, C. R., & Waters, P. J. (1999). Monogenic traits are not simple: Lessons from phenylketonuria. *Trends in Genetics*, 15(7), 267–272. [https://doi.org/10.1016/S0168-9525\(99\)01761-8](https://doi.org/10.1016/S0168-9525(99)01761-8)
- Serrano, M., de Diego, V., Muchart, J., Cuadras, D., Felipe, A., Macaya, A., Velázquez, R., Poo, M. P., Fons, C., O'Callaghan, M. M., García-Cazorla, A., Boix, C., Robles, B., Carratalá, F., Girós, M., Briones, P., Gort, L., Artuch, R., Pérez-Cerdá, C., ... Pérez-Dueñas, B. (2015). Phosphomannomutase deficiency (PMM2-CDG): Ataxia and cerebellar assessment. *Orphanet Journal of Rare Diseases*, 10(1), 138. <https://doi.org/10.1186/s13023-015-0358-y>
- Studier, F. W. (2014). Stable expression clones and auto-induction for protein production in *E. coli*. In En Y. W. Chen (Ed.), *Structural*

- genomics: General applications (pp. 17–32). Humana Press. https://doi.org/10.1007/978-1-62703-691-7_2
- Thiel, C., Lübke, T., Matthijs, G., von Figura, K., & Körner, C. (2006). Targeted disruption of the mouse phosphomannomutase 2 gene causes early embryonic lethality. *Molecular and Cellular Biology*, 26(15), 5615–5620. <https://doi.org/10.1128/MCB.02391-05>
- Van Schaftingen, J. (1995). Phosphomannomutase deficiency is a cause of carbohydrate-deficient glycoprotein syndrome type I. *FEBS Letters*, 377(3), 318–320. [https://doi.org/10.1016/0014-5793\(95\)01357-1](https://doi.org/10.1016/0014-5793(95)01357-1)
- Vals, M.-A., Morava, E., Teeäär, K., Zordania, R., Pajusalu, S., Lefeber, D. J., & Öunap, K. (2017). Three families with mild PMM2-CDG and normal cognitive development. *American Journal of Medical Genetics, Part A*, 173(6), 1620–1624. <https://doi.org/10.1002/ajmg.a.38235>
- Vega, A. I., Pérez-Cerdá, C., Abia, D., Gámez, A., Briones, P., Artuch, R., Desviat, L. R., Ugarte, M., & Pérez, B. (2011). Expression analysis revealing destabilizing mutations in phosphomannomutase 2 deficiency (PMM2-CDG): Expression analysis of PMM2-CDG mutations. *Journal of Inherited Metabolic Disease*, 34(4), 929–939. <https://doi.org/10.1007/s10545-011-9328-2>
- Verheijen, J., Tahata, S., Kozicz, T., Witters, P., & Morava, E. (2020). Therapeutic approaches in congenital disorders of glycosylation (CDG) involving N-linked glycosylation: An update. *Genetics in Medicine*, 22(2), 268–279. <https://doi.org/10.1038/s41436-019-0647-2>
- Vilas, A., Yuste-Checa, P., Gallego, D., Desviat, L. R., Ugarte, M., Pérez-Cerdá, C., Gámez, A., & Pérez, B. (2020). Proteostasis regulators as potential rescuers of PMM2 activity. *Biochimica et Biophysica Acta (BBA)—Molecular Basis of Disease*, 1866(7), 165777. <https://doi.org/10.1016/j.bbadis.2020.165777>
- Vuillaumier-Barrot, S., Barnier, A., Cueur, M., Durand, G., & Seta, N. (1999). Characterization of the 415G>A (E139K) PMM2 mutation in carbohydrate-deficient glycoprotein syndrome type Ia disrupting a splicing enhancer resulting in exon 5 skipping. *Human Mutation*, 14(6), 543–544.
- Yuste-Checa, P., Brasil, S., Gámez, A., Underhaug, J., Desviat, L. R., Ugarte, M., Pérez-Cerdá, C., Martínez, A., & Pérez, B. (2017). Pharmacological chaperoning: A potential treatment for PMM2-CDG. *Human Mutation*, 38(2), 160–168. <https://doi.org/10.1002/humu.23138>
- Yuste-Checa, P., Gámez, A., Brasil, S., Desviat, L. R., Ugarte, M., Pérez-Cerdá, C., & Pérez, B. (2015). The effects of PMM2-CDG-causing mutations on the folding, activity, and stability of the PMM2 protein. *Human Mutation*, 36(9), 851–860. <https://doi.org/10.1002/humu.22817>

SUPPORTING INFORMATION

Additional supporting information can be found online in the Supporting Information section at the end of this article.

How to cite this article: Segovia-Falquina, C., Vilas, A., Leal, F., del Caño-Ochoa, F., Kirk, E. P., Ugarte, M., Ramón-Maiques, S., Gámez, A., & Pérez, B. (2022). A functional platform for the selection of pathogenic variants of PMM2 amenable to rescue via the use of pharmacological chaperones. *Human Mutation*, 1–13. <https://doi.org/10.1002/humu.24431>